

Article

Analyzing Experimental Design and Input Data Variation of a Vanadium Redox Flow Battery Model

Robert Weber , Christina Schubert , Barbara Poisl and Karl-Heinz Pettinger

Technology Center for Energy, University of Applied Sciences Landshut, Wiesenweg 1,
94099 Ruhstorf an der Rott, Germany

* Correspondence: christina.schubert@haw-landshut.de

Abstract: Vanadium redox flow batteries (VRFB) are a fertile energy storage technology especially for customized storage applications with special energy and power requirements. The dimensioning and control of these storages is mostly calculated beforehand using battery models in embedded simulation structures. To cover various stack designs, chemistries, application strategies and system architectures, battery simulation models should be validated with different experimental input data and thus show universal functionality. In this study the functionality of a grey box VRFB model using current, voltage and state of charge (SOC) of a 10 kW/100 kWh VRFB as input data are validated for an adapted input data set using of a 5 kW/10 kWh VRFB. This model is designed for stationary applications of VRFB only. The contribution of this study is (i) to apply a suitable SOC conversion method to the raw data from the used 5 kW VRFB system, (ii) to adapt the modeling code for broader use and integration of the SOC conversion, (iii) to validate the functionality and (iv) to investigate the influence of constant current and constant voltage phases in the raw data on the accuracy of the model. A comparison of experimental data between different redox flow batteries shows that most VRFB measure the open circuit voltage (OCV) to calculate the SOC of the battery. Using the calculated SOC as an input data the proposed simulation model need to be adapted and a method is applied to use OCV input data for model validation. Although simulation models in general often assume linearity between SOC and OCV, the study showed sufficient accuracy using polynomial fitting of second order. Applying a parametrization process the results of the simulation model are compared to the raw data and the scope of application of the grey box VRFB model is defined. While using the dominant constant current phase for the charging and discharging cycle, the grey box simulation model has been sufficiently parametrized and validated for adapted input data.

Keywords: vanadium redox flow battery; redox flow battery; modeling; energy storage; grey box simulation model; validation process; energy system simulations; model parametrization; applications; state of charge; open circuit voltage; conversion methods



Citation: Weber, R.; Schubert, C.; Poisl, B.; Pettinger, K.-H. Analyzing Experimental Design and Input Data Variation of a Vanadium Redox Flow Battery Model. *Batteries* **2023**, *9*, 122. <https://doi.org/10.3390/batteries9020122>

Academic Editors: Pascal Venet, Karim Zaghbi and Seung-Wan Song

Received: 23 December 2022

Revised: 20 January 2023

Accepted: 3 February 2023

Published: 9 February 2023



Copyright: © 2023 by the authors. Licensee MDPI, Basel, Switzerland. This article is an open access article distributed under the terms and conditions of the Creative Commons Attribution (CC BY) license (<https://creativecommons.org/licenses/by/4.0/>).

1. Introduction

With increasing focus on the energy turnaround, the amount of renewable energy (RE) has been growing for decades [2]. The Framework Convention decided at the World Climate Conference in Glasgow in 2021 favors the use of RE, as fossil energy production is to be reduced, especially as the CO₂ neutral energy production offers the decisive advantage to achieve the global climate goals until 2030 [3].

This evolution raises new technical and economic challenges that have to be considered when integrating RE into the existing grid. In fact, there is a decentralization of energy production in the utility grid, which is exposed to fluctuations due to the inconstant and unpredictable source of energy. Thus, there is increasing interest in systems for voltage and frequency stabilization and reduction of load peaks to ensure the stability of the grid [4].

The VRFB is a promising energy storage technology, which has been researched and developed since the 1970s [5,6]. Due to its independent scalability of power and energy

as well as the modular design, it is highly attractive for stationary applications [5–8]. To achieve a high efficiency and long lifetime, the placement and control in the grid has a significant importance [9]. For this purpose, simulation models are used in advance to predict the batteries' behavior in different applications, control or placement strategies [9].

Simple simulation models help to implement the characteristics of energy storages, their control algorithms and placement into embedded energy architectures. Generally, the scope and modeling approaches for battery simulations define the input data structure. Input data are defined as the raw data collected from the battery systems, which can start from full charging/discharging cycles as easy accessible data to equivalent resistances or even material compositions and kinetics on a more detailed level. The modeling scope itself can result in limiting the experimental design and input data used for the simulation model, as detailed material compositions may not be used for application-oriented modeling. Reversibly, electrical connections and model integration into general system architectures such as grids might not be used while comparing stack designs or chemistries. Thus, battery models can only be universally applied to defined modeling scopes.

The original model proposed in [1] has been developed for the purpose of system analysis and coupling the battery with different application-oriented simulation levels in future grid scenarios. Thus, the applicability of the model is restricted to stationary storage and cannot be applied to other storage technologies, such as metal-ion batteries (e.g., lithium-ion batteries). The original simulation model is a grey box model dedicated to researchers with no access to the VRFB container system itself. The assumption has been made that detailed input data on materials, resistances or chemistries is not available to the end user, such as system integrators or grid operators [1]. The experimental design used to elaborate the model is based on five charging and discharging cycles at different power and defined SOC ranges from 20 to 80%. More accurate measurements, e.g., impedance spectroscopy or UV/VIS analysis of the electrolyte, cannot be made with these systems without the loss of guarantee. Thus, the grey box model can be parameterized with a low amount of easy accessible measurements. The input data structure is based on the measured output of one specific 10 kW/100 kWh VRFB. The model requires standardized measurement data, which may differ depending on the battery system considered. By analyzing another VRFB system, it has become clear that a change in experimental design necessitates a model adaption.

The aim of this work is to investigate the effect of input data variation on the functionality as well as the programming and thus validate the model presented in [1]. Input data variation describes the difference between the battery system which was used during the development process and the battery for the validation. Therefore, the experimental design of two different VRFB is compared and a method for data conversion of the SOC from primary sensor data is applied. Afterwards, the model validation is performed to verify the model prediction capabilities. Independent functionality and sufficient accuracy between raw and simulated data is pursued while maintaining the differential-algebraic model.

The remainder of this paper is organized into three sections: starting with a short introduction of the functionality of the existing model, Section 2 discusses the experimental design between different VRFB systems and the effect on the model. Furthermore, the sections show methods to identify the SOC of VRFB and concludes the method used for the course of the study. Section 3 presents the results of the data conversion, the model parameterization and validation of the model prediction. Section 4 concludes the paper and highlights open challenges and future research directions.

2. Materials and Methods

2.1. Grey Box VRFB Model

In this study, the functionality of the grey box VRFB model proposed in [1] using current, voltage and SOC of a 10 kW/100 kWh VRFB as input data is validated for an adapted input data set using of a 5 kW/10 kWh VRFB. To enable universal functionality independent of the input data set used, this study analysis the experimental design used to simulate

the behavior of a VRFB in [1] and shows how to adapt the model in case the experimental input data differs.

Figure 1 shows the simulation steps one to four as proposed in [1]. Starting with the raw data extraction (step 1) of constant power charging and discharging cycles measured by the Battery Management System (BMS) the data are modified to smooth peaks, delete zero values and reduce the step size for the following optimization routine (step 2). Afterwards, the raw data are used in two different ways (steps three and four). As specific battery-related parameters has been not accessible for the model description from the raw data, a parametrization routine is applied. The parametrization process (step three) enables optimal values for current losses, theoretical storage capacity, OCV, and ohmic cell resistance based on the experimental data.

The model itself is based on one differential and two algebraic equations, calculating SOC, voltage and DC power. Starting with defined start values for current losses, OCV, and ohmic cell resistance, a screening range is applied for the parameter theoretical storage capacity. The simulation error for the state variables current, voltage and SOC is calculated for every time step and every screening parameter of the theoretical storage capacity. The screening range as well as the start parameters are adapted during three consecutive optimization routines. The goal is to achieve the lowest possible error between the raw data and the simulated data for voltage, current and SOC. Afterwards the optimized values for current losses, theoretical storage capacity, OCV, and ohmic cell resistance are stored. During the optimization process, the amount of raw data used can be adapted, e.g., reducing the data from five total cycles to three. In the last step four, the model is validated for different charging and discharging cycles and time dependent curves can be investigated.

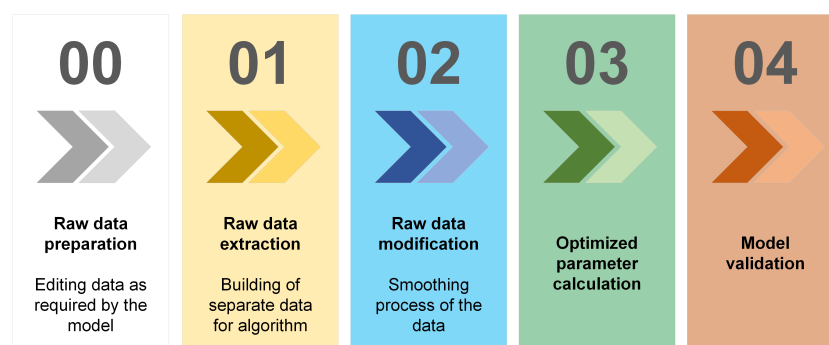


Figure 1. Method of the simulation model with steps one to four as proposed in [1] and extended raw data preparation step zero.

For the investigation of universal functionality as well as experimental design in this study step zero has been added to the simulation model. The changes in the battery model itself, as well as the raw data preparation, will be explained in the following chapters.

2.2. Comparison of the Experimental Design

The simulation model used by Zugschwert [1] was developed using data from a Cell-Cube FB10-100 VRFB, hereafter referred to as Battery 2. The new data set of this research work was obtained from a battery system called Volterion VRFB 11, hereafter referred to as Battery 1. In the process of validating the model, it is necessary to adapt the newly recorded data sets of Battery 1 to the data schematics of the simulation model. Table 1 describes the two batteries with respect to their dimensions and most significant characteristics. Generally, redox flow batteries can be either current- or power-controlled.

Table 1. Overview: Comparison of the preset parameters of the simulation model.

	Battery 1	Battery 2
Model name	Volterion VRFB 11	CellCube FB 10–100
Stack configuration	2 stacks	10 stacks
Nominal power	5 kW	10 kW
Overall capacity	10 kWh	100 kWh
Nominal voltage	48 V	48 V
Considered SOC boundaries	20–80%	20–80%
Temperature range	0–40 °C	20–30 °C

Battery 1 has a nominal power of 2.5 kW per stack, with a maximum capacity of 10 kWh at 48 V DC operating voltage. However, it should be noted that a power value above 2 kW was never tested. In the work, the operation SOC range is specified between 20% and 80%, which corresponds to an OCV of 1.24 V (20%) and 1.45 V (80%) [10]. The SOC boundaries are identical to that of Battery 2 and therefore correspond to the simulation model [11].

Battery 1 is current-controlled, which is one of the significant differences to Battery 2. The energy storage system can be operated with a constant current, which means an inconstant power level during charge and discharge. During charging, when the stack voltage increases steadily at a given constant current, this results in a constant increase in power. The losses of a VRFB can be classified into coulombic, voltaic and electrical losses. The electrical losses include auxiliary consumers such as the pumps. In addition, a bidirectional AC/DC converter is installed, which converts the voltage during the charging process from the input AC voltage to the output DC voltage. The bidirectional DC/DC converter located between the VRFB and the AC/DC converter adapts the DC voltage to the battery or the AC/DC converter system. Furthermore, temperature sensors are installed, which allow monitoring of the various areas and components of the battery [11].

Battery 2 has a nominal power of 10 kW, with a maximum capacity of 100 kWh consisting of 10 stacks with a nominal voltage of 48 V. The VRFB is power-controlled and is operated in a SOC range of 20 to 80%. The stacks are connected via three bidirectional AC/DC converters. In contrast to Battery 1, this battery has a ventilation system which, together with the pumps, is connected to an additional 24 V DC power supply on the primary side of the AC/DC converter [12].

2.3. Comparison of Input Data Setup

The measurement data of Battery 1 are collected over the period of one charge and discharge cycle varying current from 15 to 35 A, with a defined window of SOC from 20 to 80%. Thus, five measurement series starting with 15 to 35 A are available for the subsequent modification of the data sets.

The simulation model defines the input data structure. During the development of this model, only data from Battery 2 has been used. Based on this, the input data and the further calculation of the simulation model are specified. Therefore, the model is not universally applicable for any VRFB raw data without restrictions. As the BMS from different manufactures provides different types of data, the analysis of the experimental design as well as the input data variation are a necessary step to enhance model usage. The SOC input data can be used as an example. While the BMS of Battery 2 records the SOC, this value is not available by the BMS of Battery 1. At the latter, it is necessary to use a conversion method to convert the OCV to obtain the SOC of the battery. In Battery 2 there is no access to every single data input of the BMS, but only the mathematical transformation to SOC values in percent. This results in differences between the data from the battery and the simulation model, rendering the data useless for Battery 1. The conversion of the data designed in this work will finally allow the simulation model to be parameterized.

Table 2 shows the data required by the simulation model. The numbering corresponds directly to the order in which the data must be placed in the columns. The data sets

of Battery 1 on the right side serve to illustrate the differences to the simulation model. These must be converted afterwards by appropriate methods in order to be able to execute the validation of the model.

Table 2. Overview: Comparison of the preset parameters of the simulation model.

Number	VRFB Simulation Model	Battery 1 Data Set
1	Absolute time [s]	Time stamp [hh:mm:ss]
2	Grid side power AC [W]	-
3	SOC [%]	-
4	Total stack voltage [V]	Voltage per stack [V]
5	Total stack current [A]	Current per stack [A]
6	Temperature [°C]	-

In the following, an explanation of the parameters of the simulation model and Battery 1, which are compared in Table 2, is given:

- (1) As a basic parameter, the specification of time at measurement represents a fundamental part of the simulation model and the data set of Battery 1. Second values are needed for the simulation, therefore the data sets with specified timestamps must be converted accordingly.
- (2) The simulation model expects the measured AC power at the grid connection point. These data are required for the subsequent efficiency analysis and is only recorded for the measurement series with 15 A charge and discharge current. A defect at the converter makes further recordings impossible. The measured values recorded up to that point are not plausible. Due to the current data situation, which cannot be extended, there is no efficiency analysis and this part of the model is not used within this study.
- (3) To determine the optimization parameters, a modified formula from Nernst equation is applied, which describes the battery model as one of the three main equations. Battery 2 provides a calculated SOC through its integrated BMS, which can be passed to the simulation model. Battery 1, on the other hand, does not have this function and data, which is why several options for modifying the input data and determining the SOC were explained in the next chapter.
- (4) Differences are found in the data sets for the voltages and currents at the stacks. The model calculates with the total voltage, which represents the average voltage of both stacks. The data sets of Battery 1 only provide the individual stack voltages which would allow a simulation, but only with the voltage of one stack. Since the stacks are usually electrically connected in parallel, the voltage values differ only slightly. Thus, a mathematical adjustment of both stack voltages of Battery 1 takes place by forming the average value from both stacks.
- (5) If the total capacity of the battery is to be determined, the total current must be entered into the simulation. The data set of Battery 1 provides the current per stack, which is why a conversion is made to obtain the total current. As another part of the simulation model, a smoothing of certain raw data takes place. Unlike the raw Battery 2 data used in development, Battery 1 is current driven. The scatter of the current values of Battery 2 is therefore much smaller. However, no changes are made in this respect, since the functionality is also maintained with the raw data of Battery 1.
- (6) The simulation model offers the possibility to perform the calculations depending on the temperature value of the electrolyte. For this purpose, this value is read in via the last column of the input data set. However, since the battery system of Battery 1 does not record a temperature value, this is left out for later consideration. A constant value of 295.15 K (23 °C) is assumed for the temperature.

2.4. Methods for Obtaining the SOC

The main focus for the model adjustment is the determination of the SOC, since it is the only value that is measured differently by the two battery systems. For this purpose, different methods to obtain the SOC of a VRFB are investigated [13–17].

The most promising and commercialized approach is the dependency of SOC on OCV under known system conditions, e.g., electrolyte composition, by integrating a separate cell into the electrolyte circuits. SOC and OCV can be converted from one to the other with little variation over multiple cycles and electrolyte temperatures. In addition, the ability to count ampere-hours over the time of charging and discharging is suitable. However, deviations in the measured values reduce the accuracy. Starting from the OCV, the most accurate determination of the SOC is a discharge test. The precondition for this is that the battery is fully charged. From this point, the measurement of the quantities required for the calculation begins [16].

The following describes each method briefly and show utilization potentials for the model validation performed within this study.

2.4.1. Discharge Test

Discharge tests are performed for fully charged batteries (SOC = 100%) to determine the continuous SOC based on the remaining capacity. Yet, it is difficult and prone to error to clearly define SOC boundaries, as this depends strongly on the electrolyte used [9,17–20]. Determination of SOC boundaries can be made, among other things, by using a separate OCV cell or UV–Vis spectroscopy of electrolyte [17,20]. The latter is time-consuming as the information obtained is only valid for this point in time and continuous repeating is necessary, which makes it a very costly method [17,20].

If starting points are clear, remaining capacity and thus SOC can be determined using continuous discharge time and the discharge current. This test is performed under known system conditions in order to be able to make reliable statements about the remaining capacity, is very time-consuming, and cannot be performed while the battery is in operation [14]. Since a SOC determination at least for starting values must be made during the measurement process, this option is not to be considered for the model validation in this study.

2.4.2. Ampere Counting

Ampere Counting represents the most cited method in the literature. Formula (1) describes the increase in SOC over time as the integral of the current $I(t)$ per time step in relation to the total capacity C_0 [14]. The total capacity C_0 in Ah equals the nominal capacity as listed in the data sheet in the optimal case. In practice, this value differs from the theoretical one due to, e.g., cross-over phenomena between the vanadium species [16]. To obtain the real capacity discharged, tests as stated above need to be performed before Ampere Counting can be applied. This procedure guarantees accurate capacity prediction.

$$SOC(t) = SOC_0 + \frac{\int_0^{\Delta t} I(t) dt}{C_0} \quad (1)$$

$$SOC(t) = SOC_0 + \frac{\int_0^{\Delta t} I(t) - I_{Loss} dt}{C_{Stor}} \quad (2)$$

This study refers to a simulation model using the fitting parameter C_{Stor} as the real storage capacity instead of performing discharge tests before every measurement. The adapted Formula (2) represents the differential equations used in the simulation model. Furthermore, a second fitting parameter I_{Loss} is used within the simulation model to take current losses due to internal processes e.g., shunt currents into account. The use of the theoretical values without further corrections for $I(t)$ and C_0 leads to inaccuracies in the

determination of the SOC(t) between the model and the raw data. These inaccuracies are added up over the measurement or even battery run time, leading to a disadvantage in the SOC determination which is difficult to reconstruct within the model. For that reason, the SOC method Ampere Counting has been identified as not suitable for this study.

2.4.3. SOC–OCV Relation

The OCV can be calculated using the modified Nernst equation presented in [15]. Further simplifications, presented in [17,18,21–23], relate the SOC to the quotient of the respective vanadium ion concentration (c_{V2+} , c_{V3} , c_{V4} , c_{V5}) and the overall vanadium concentration c_V (Equation (3) and (4)). The theoretical equation to calculate the OCV is summarized in Equation (5) and corresponds to the algebraic equation used in the simulation model [1]. The Faraday constant F , the universal gas constant R , the average temperature T in Kelvin, the amount of cells per stack N_{cell} and the amount of electrons transferred during the reaction $z = 1$ are used within the equation.

$$SOC_c = \frac{c_{V2}}{c_V} = \frac{c_{V5}}{c_V} \quad (3)$$

$$1 - SOC_c = \frac{c_{V3}}{c_V} = \frac{c_{V4}}{c_V} \quad (4)$$

$$U_{Stack} = N_{cell}U'_0 + \frac{N_{cell}RT}{zF} \log \left[\frac{SoC^2}{(1 - SoC)^2} \right] \quad (5)$$

To apply the SOC–OCV relation, the OCV is measured by including a separate open circuit cell into the hydraulic circuit of the VRFB. As described in Section 2.3, the original raw data used for the simulation model were based on SOC values calculated by the BMS of Battery 2 [1], whereas the raw data of this study (Battery 1) shows OCV values without direct conversion to the SOC. With reference to Equation (5), the OCV measurement is only reliable if the electrolyte is not influenced by cross-over phenomena or irreversible side reactions [17,18]. The latter cannot be compensated by the rebalancing system and reduce the theoretical capacity of the battery [17–20]. Thus, influencing the quality of SOC prediction over the lifetime [9,17–20].

The continuity of the OCV–SOC relation is important for the simulation model. Due to the algebraic equations used, the internal electrochemical phenomena are described using a linear approximation and the model is not able to predict non-linearities in the voltage profile correctly [1]. As shown in Figure 2, non-linearities in the voltage profile occur at the beginning and end of the charging and discharging process. Linearity between the OCV and the SOC has been reported in literature within the ohmic phase of the voltage profile [24]. As the ohmic phase occurs only between specific ranges, the linearity is limited. Depending on the investigated literature studies, these limits can be found between 10% and 95% SOC [24].

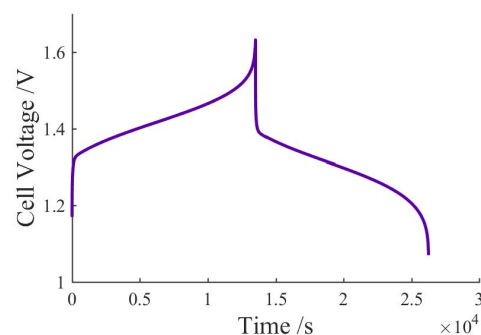


Figure 2. Simulated theoretical cell voltage of a VRFB between 1% and 99% SOC.

As the SOC–OCV correlation is the most promising method to generate the required input data for the simulation model, mathematical fitting needs to be applied to the raw data of Battery 1. The manufacturer’s specifications set the SOC–OCV limits between 20%

and 80% corresponding to OCV of 1.24 V (20%) and 1.45 V (80%) [10]. Since the start for the calculation is at a SOC of 20%, the manufacturer’s specification for the OCV is necessary for the correlation process. Therefore, the overall result is distorted in case of unknown changes in the vanadium concentration due to cross-over or side reactions and the manufactures OCV–SOC relation limits might not represent the voltage profile correctly. The following chapter show the results for the mathematical fitting of SOC and OCV for Battery 1 as well as the model validation with the complete input data set.

3. Results and Discussion

3.1. OCV–SOC Conversion Results

The following chapter shows the conversion of the OCV to the SOC values of Battery 1 using different regression methods. In the first step, a linear regression is applied to the OCV measurements for different cycles between 15 A and 35 A. The parameters of the regression lines were calculated using Matlab numerical software. For this purpose, the command *polyfit* with specification of the polynomial degree 1 is applied. The comparison of the measurement data and the regression line for 15 A and 35 A is displayed in Figure 3a,b. Shown in blue, the measured points represent the SOC over the OCV for different preset charging currents. Shown in black are the calculated regression lines, which are determined by linear fitting.

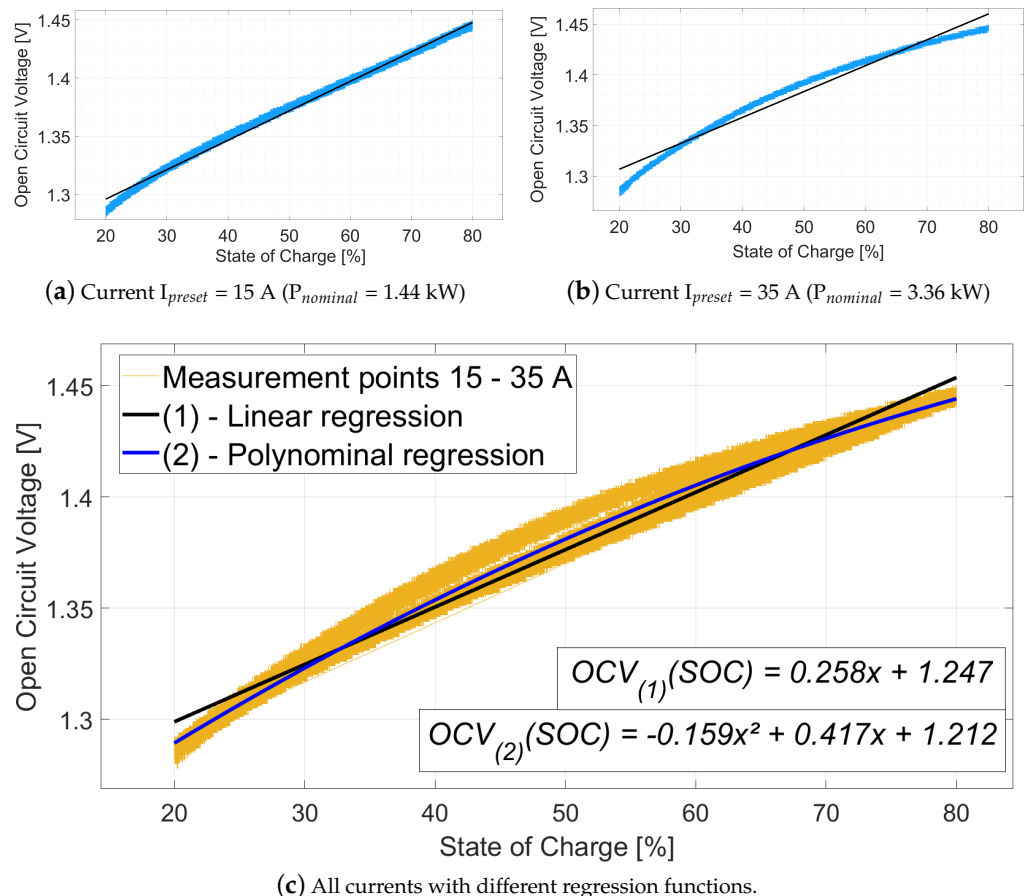


Figure 3. OCV–SOC relation results: (a) I_{preset} 15 A; (b) I_{preset} 35 A; (c) data points of all measurements from I_{preset} 15 A to 35 A and different regression functions.

In Figure 3a good proportionality characteristics can be identified in a first approximation. At the upper end of the SOC boundary, the measurement points are congruent with the regression line. The proportional behavior becomes increasingly worse at the lower limit of the SOC, where potentially non-linear activation overpotentials occur. Within the

SOC of 20 to 24%, the measured values and the regression line are no longer congruent, with a discrepancy of 0.014 V of the OCV. By increasing the current from 15 to 35 A the OCV is increasingly inadequately mapped at the lower limit as well as the upper limit of the SOC and a parabolic shape becomes increasingly apparent. With the highest possible current of 35 A, the curved-shape of the blue measured values is at a maximum. The regression line is only congruent with the linear function in the range from SOC 28.3 to 35.9% and from 60.8 to 71.2%. This equates to a percentage error of 2.68%. The error between the regression line and the calculated single points in the middle of the SOC range is 0.013 V.

In order to quantitatively evaluate the change in slope and axis intercept of the linear equations for all available currents, these and the corresponding OCV values at 20% and 80% are summarized in the table below:

The given linear equations show that the current has no significant effect on the slope and the intercept. The limit of the OCV at 20% marginally rises with increasing current, but can be omitted from consideration at a maximum difference of 0.011 V. The maximum difference of SOC₈₀ among the measured OCV with different charging currents is 0.012 V. In the direct comparison of the deviations of the OCV of SOC₂₀ and SOC₈₀ occurring between one another, the difference is 0.001 V. The results from the previous figures and the table of linear equations indicate that there is no shift in the OCV–SOC dependence, only a curvature that needs to be corrected. The model itself can represent the OCV–SOC relation properly using a linear approximation. To enhance the OCV prediction itself, it is recommended to evaluate the electrolyte imbalance during the battery operation and use a rebalancing system. Thus, battery functionality and state of health are preserved. In case electrolyte imbalance occurred, OCV borders applied to the battery control can shift and SOC prediction can be increasingly inaccurate. A shift within the OCV values does not change the characteristic shape of the OCV, which is mapped by the simulation model. The model itself can represent the OCV–SOC relation properly, even if imbalances shift the SOC range. SOC boarder can be adjusted to values beyond 20 to 80%.

The simulation model has to be universally applicable for all preset currents after one-time parameterization [1]. In the second step, all previously measured points are summarized in yellow in Figure 3c. The linear regression line, calculated from the all OCV measurement points, is shown in black. It forms the mean values of the linear equation previously shown in Table 3. However, the absolute level of the OCV values at the borders has still remained unconsidered. The manufacturer of Battery 1 specifies an OCV of 1.29 V at 20% and 1.45 V at 80% SOC [10]. With the linear function, SOC₂₀ is 1.299 V and SOC₈₀ is 1.453 V, which are within the manufacturer’s measurement tolerance. Compared to the yellow point cloud, however, the straight line does not show an optimal shape. Therefore, we switch from linear regression to polynomial regression in the third step. With polynomial degree 2, shown in blue color in Figure 3c, the SOC–OCV correlation is improved. The limits are 1.294 V for SOC₂₀ and 1.464 V for SOC₈₀ and these voltages are still within an optimal range. Thus, the conversion of the OCV to the SOC is carried out using the function with degree 2, which minimizes the error caused by this calculation operation.

Table 3. Parameters after linear regression of the individual measurement tests.

Preset Charge and Discharge Current	Linear Equation	OCV at 20% SOC	OCV at 80% SOC
15 A	$OCV_{(SOC)} = 0.253x^2 + 1.245$	1.296 V	1.448 V
20 A	$OCV_{(SOC)} = 0.260x^2 + 1.243$	1.295 V	1.451 V
25 A	$OCV_{(SOC)} = 0.260x^2 + 1.243$	1.296 V	1.456 V
30 A	$OCV_{(SOC)} = 0.258x^2 + 1.253$	1.395 V	1.459 V
35 A	$OCV_{(SOC)} = 0.256x^2 + 1.247$	1.307 V	1.460 V

3.2. Parametrization and Optimization of the Redox Flow Model

The following chapter shows results from each modeling step: raw data extraction (1), raw data modification (2), optimized parameter calculation (3) and model validation (4). The fitting parameters total capacity (C_{Stor}), current loss (I_{Loss}), cell resistance (R_i) and cell voltage (U_0) are optimized following the mathematical approach in [1]. After successfully parameterizing the model, the accuracy between the model and the raw data is validated.

3.2.1. Raw Data Extaction

Due to the existing simulation model, major differences are occurring between the raw data and the actual data required for the model. The SOC limits of the simulation model are at 20% and 80%. As the grey box model from [1] is linear, it provides the most accurate values within the linear region of the status variables (e.g., SOC). Non-linearities are fitted with a linear approximation of a self-discharge current. The pauses between measurement series as well as lead times and other interruptions are removed from the raw data. Thus, discharge cycles immediately transition to charge cycles and vice versa.

Figure 4 visualizes the raw data (shown in yellow and blue) of the charging and discharging currents from 15 to 35 A, starting with the lowest preset current. Positive slopes represent the charging, the remaining ones the discharging process. Marked with the yellow gradient are those measuring points which are actually used in the simulation model. The limits at which the model should cut off the data are marked by black horizontal lines at 20% and 80% on the y-axis of the figure.

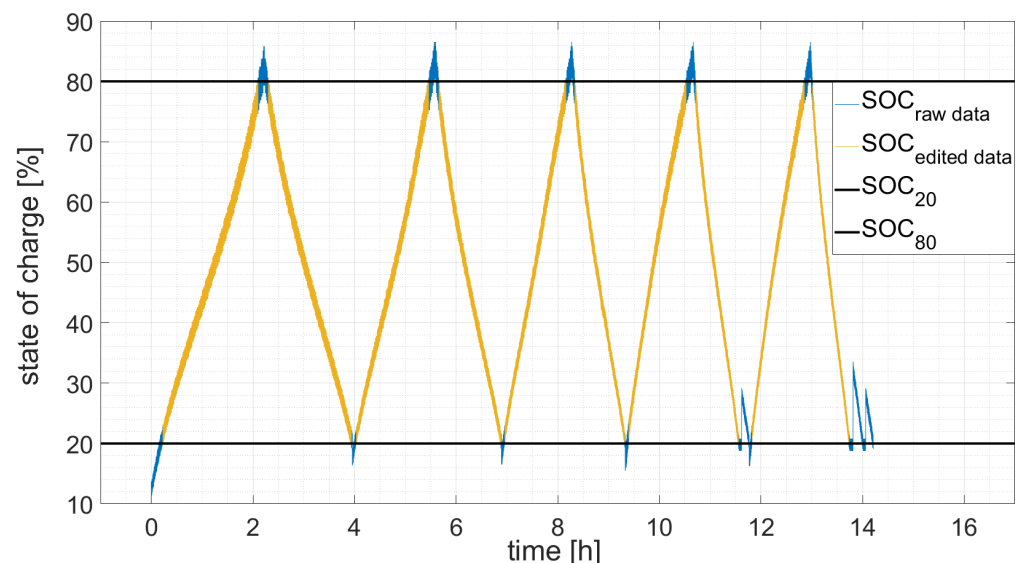


Figure 4. Visualization of the original and edited data from the simulation model.

Validations between the original source code published in [1] and the now modified source code allow the first data set to be used independent of charging or discharging. Thus, the data of the first charging cycle (hour 0 to 1.25) are included in the later parameterization. The measurement failures occurring at hour 8.6; 14.4 and 14.6 express themselves in jumps and are automatically excluded.

3.2.2. Raw Data Modification

In the next step, the raw data for SOC, voltage, and current is modified and values are smoothed. This reduces the total data points for the following optimization routine to 20 values and thus saves calculation time. Consequently, the information from SOC and the stack voltage is also limited to the same number. Representative for all recorded charging and discharging processes, the following figures preset the smoothing of three parameters; SOC, stack voltage and charge current for the 30 A cycle.

The left side of Figure 5a shows in blue fluctuations due to the SOC–OCV conversion. The fluctuations increase slightly up to 3% as the SOC increases. The smoothed values, consisting of a total of 20 individual points, are shown in yellow. Due to the generally small fluctuations of the raw data, the straight line from the smoothed values does not represent a large deviation from the original data.

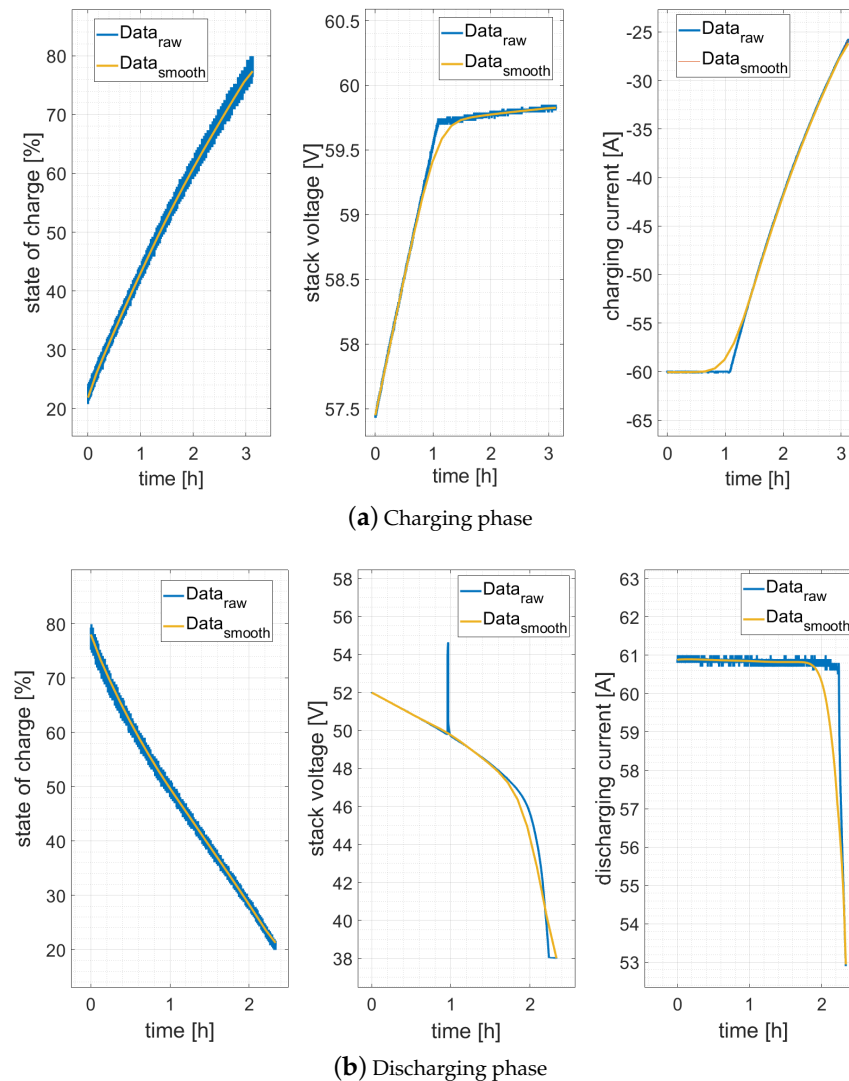


Figure 5. Comparison of the raw data and modified data of the 30 A cycle for the: (a) charge phase; (b) discharge phase.

The blue line in the middle of Figure 5a shows the raw data of the stack voltage over time. During charging, the stack voltage has a proportional behavior in the range from 57.45 to 59.05 V. After that, the transition from Constant Current (CC) to Constant Voltage (CV) takes place, which can be seen by the turn after hour 1.1. Shown in yellow are the smoothed values, which only deviate from the raw data in the flattening transition to CV (hour 1.1) until its end. The discrepancy here is 0.2 V.

The figure on the right describes the current of the charging process, indicated by the negative signs with a maximum 60 A for two stacks. Contrary to the power-controlled Battery 2, Battery 1 is current-controlled, thus a smaller fluctuation of the current value is noticeable (c.f. Section 2.2). Therefore, the smoothing function in the current curve represents a very small deviation. During the CC phase, a constant current with fluctuations of less than 0.3 A has been identified.

Figure 5b illustrates the discharge process in contrast to the previous Figure 5a. The fluctuations in SOC in blue are similar to those of the charging process. The duration of the two processes is different, as the discharge time is around half an hour shorter than the charging time.

In the discharge phase, proportionality of the stack voltage (middle figure) prevails in the range from 51.90 to 48.70 V, whereby the voltage peak at one hour is to be neglected, since it occurred due to a measuring device error. If the battery reaches the SOC value of 36.94%, the voltage decreases faster. The smoothed curve is almost identical to the measured values in the period from the start point to hour 1.5. With rising slope (hour 1.5 to 2.5) the modified data deviates from the raw data. The maximum deviation occurs at hour 2.2 with a value of 2.1 V.

The right diagram of Figure 5b shows the sum of the currents of both stacks over time. These current fluctuates in a range of 0.3 A, which is corrected by the smoothing function. In the period from hour 0 to 2.2, the battery discharges with constant progression. In this range, the voltage decreases from 60.7 to 52.9 A up to the end of the discharging process. As in the stack voltage, the course of the raw data coincides with the smoothed data over the entire course, except at the time when the current values start to decrease. The maximum difference between the original and smoothed data is higher than 3.93 A after 2.2 h, which corresponds to a deviation of 6.49%. Overall, the fluctuations in the raw current values increase with increasing currents.

Using the smoothed data, the optimization process, presented in the following chapter, calculates optimal values for the fitting parameters total capacity (C_{Stor}), current loss (I_{Loss}), cell resistance (R_i) and cell voltage (U_0).

3.2.3. Calculating the Optimization Parameters

Due to the modified battery system and raw data, changes take place in the starting conditions for the optimization steps and their step size. The selection of the realistic initial values is essential for the optimization of the simulation model. The cell voltage, total capacitance, current losses and cell resistance are the four optimization parameters. The loop index and the step size influence the accuracy of the optimized parameters, as these parameters define the frequency of the model calculation.

These adjustments present themselves as an iterative process and the re-adjustment of start parameters takes place as often as necessary until suitable values are found. Especially, the total capacity (C_{Stor}) plays an important role, as will be shown in more detail later. The calculation of the start parameters provides a good starting point for the iterations of the parameter optimization. The former and new initial values and step sizes are shown in the following Table 4.

Table 4. Comparison of the preset parameters of the simulation model.

	Current Values [1]	New Values
Total capacity C_{Stor} [As]	8,700,000 (2416.67 Ah)	1,000,000 (277.78 Ah)
Current loss I_{Loss} [A]	10.0	2.0
Cell voltage U_0 [V]	1.375	1.2
Cell resistance R_i [Ω]	0.00075	0.0010
Loop index [%]	5	50
Step size k [-]	30	30

The total capacity is calculated using the data from the data sheet of Battery 1. With a total capacity of 10 kWh and an average measured stack voltage (36 V), the capacity C_{Stor} of the battery is calculated. As the leakage current is an optimized value representing internal electrochemical phenomena, it can not be measured by sensors. The theoretical cell voltage cannot have a large deviation from the original value of Battery 2, as both systems are based on vanadium electrolyte. The start value of the cell voltage is therefore set only a minimum lower than the previous value. After the first

attempts of optimization, a slightly higher value for the internal resistance R_i and for the capacity C_{Stor} is obtained and the starting value is slightly increased. While the calculated battery capacity from the manufacturer is set to 10 kWh (208.33 Ah, 48 V), the optimized start value is set 25% higher. Due to some iterations in advance, the initial value of C_{Stor} changes from previously 749,988 As (208.33 Ah) to 1,000,000 As (277.78 Ah).

The step size, on the other hand, has a large influence on the screening range of the capacity during the iterations. To determine the smallest possible error between model and raw data, the screening range and thus the resolution is increased from 5 to 50% for this study. The step size remained at the original value. An automation or calculation of the step size and the loop index is not possible. For this, a minimum of the model error must be found, without exact knowledge about its position.

According to the simulation model explained by [1], three optimization iteration steps take place. These are marked in Figure 6 by s1 to s3. These steps are used to minimize the deviation error between model and raw data for different values of C_{Stor} . As the error calculation is based on the method of the least square sum (LSS) and is added for all state variables (current, voltage, and SOC) it is unitless. The first two iterations s1 and s2 occur with a fixed step size, while s3 changes depending on the step size parameter.

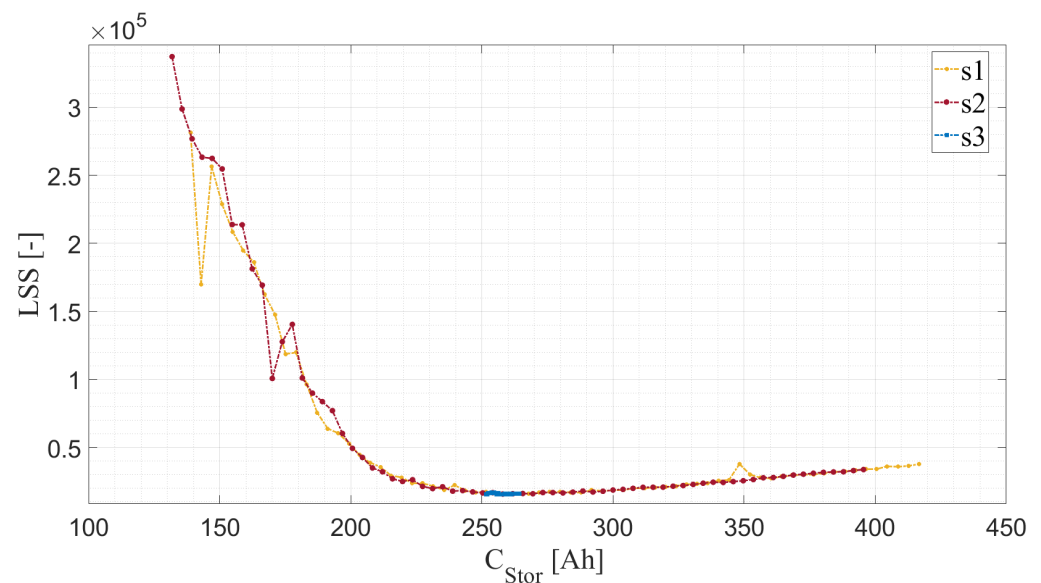


Figure 6. Finding the local minimum of the parameter C_{Stor} after the three optimization steps.

The progress of LSS within the screening range of C_{Stor} during s1 is illustrated in yellow in Figure 6. The simulation model is given an initial value for the screening range of C_{Stor} , which represents the theoretically possible capacity of the battery system. The loop index $k_{C_{Stor}}$ is used to set the resolution of the screening as a percentage of the start value. In the case of the first battery system, this extends from 138.5 Ah to 415 Ah (starting value = 277.77 Ah; $k_{C_{Stor}} = 0.5$). In general, the reduction of the step size causes an increase of the scan range.

The blue data points in Figure 6 indicate the local minimum of the C_{Stor} between 250 Ah and 275 Ah. In step s3, the model error (LSS) is minimized from initially 28,000 to around 16,000. After completion of the three steps, the local minimum is calculated at a value of C_{Stor} of 255.66 Ah.

The results do not show a Gaussian bell curve shape for the optimization steps, as the original results of the dissertation by Zugschwert using Battery 2 might have suggested [9]. The optimization results of this study indicate a rapid left-shaped optimization, while the right side of the curve increases more slowly.

Figure 7 visualizes the third and thus most exact optimization step of the variables C_{Stor} and I_{Loss} over the preset step size of $k = 60$. For each step size the differential-algebraic equation system is solved with the respective parameters.

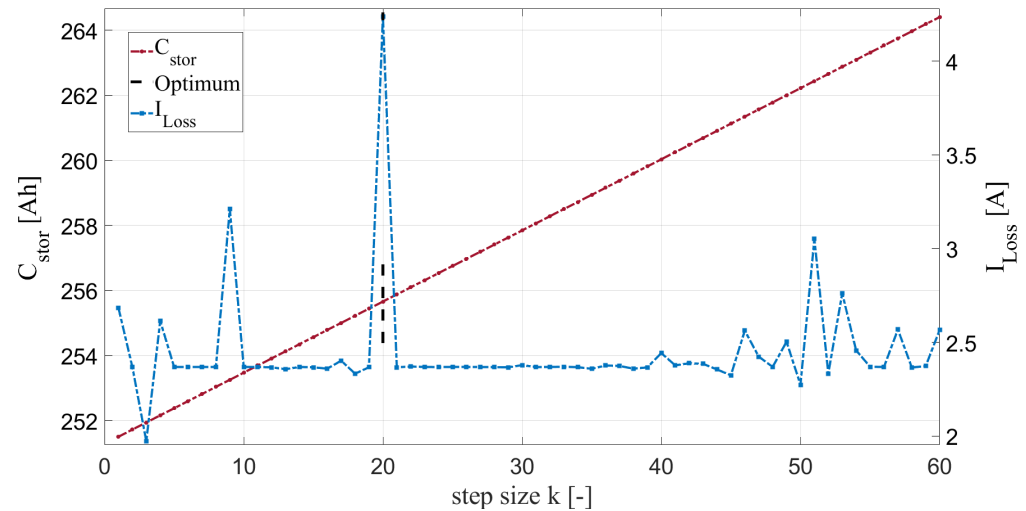


Figure 7. Third optimization step of C_{Stor} and I_{Loss} with preset step size of $k = 60$.

Due to the pre-programmed values of the C_{Stor} , its course in this figure is a linear progression (red line). With the limitation to the step size, the number of measuring points of C_{Stor} and I_{Loss} is also limited to 60 values. For the fitting parameters (internal resistance R_i , cell voltage U_0 , current losses I_{Loss}) an optimization function is used to solve the differential-algebraic equation system with a minimal LSS. The blue line shows the progress of the current losses I_{Loss} over the step width. The vertical black dashed line shows the minimum of the calculated model deviation. During the screening range the value I_{Loss} ranged from 1.97 to 4.24 A. The value with the smallest deviation from I_{Loss} is 4.24 A. Associated with this is the smallest error of C_{Stor} at a value of 255.66 Ah. The latter is a battery-specific value and is lower than the manufacturer's value due to various factors. These include the reduction in capacity due to secondary reactions.

Figure 8 shows the optimization parameters R_i and U_0 over the pre-configured step size of $k = 60$. Shown in blue is the calculation of the cell internal resistance R_i , which varies between 1.75 m Ω and 2.05 m Ω for the third optimization step. The calculated optimum is at 1.8 m Ω . The optimum of the cell voltage U_0 is set at a value of 1.33 V with.

The two parameters are mostly dependent on the battery system and hence comparable with the dissertation of Zugschwert [9]. By considering single cells, the starting and optimum values must be close to those given in the thesis. In this respect, the calculated results of the optimization parameters allow a first plausibility check. In order to check the determined internal resistance R_i and the cell voltage U_0 , the optimum parameters calculated in Figure 8 with 0.645 Ω and 1.376 V. are applied for the comparison. While the deviation between the thesis in [1] and this study is 155% for the internal resistance, the cell voltage is only 24.7% lower than the optimum value according to the thesis [1].

The reasons for the deviations are versatile. Zhou et al. [25] shows that the stack voltage is dependent on various parameters. These include the SOC, the current density and the flow rate. Thus, the starting parameters for determining the internal resistance are within the voltage range of 1.05 to 1.8 V. The range of application is between 10% and 90% SOC. For the selection of the start parameters, the approach is intended that the start parameters are set at the lower limit of the voltage range. This should ensure that the determination of the correct minimum takes place over the entire calculation range [25].

Moreover, the internal resistance is influenced by numerous factors and parameters. The electrode has the most influence, followed by the membrane and the electrolyte. Due to the electrolyte, the cell resistance is also dependent on the SOC [26]. Since the individ-

ual cell components are not known, only a qualitative plausibility check of the cell resistance can be performed. Recent studies provide a cell resistance between $0.87 \Omega\text{cm}^2$ and $1.5 \Omega\text{cm}^2$ [27–29]. Multiplication of the calculated value for R_i of $0.18 \text{ m}\Omega$ with the surface size of the single cell approximated with 682 m^2 , results in $1.23 \Omega\text{cm}^2$. The resistance R_i calculated by the model is in the range determined by other studies and is therefore trustworthy.

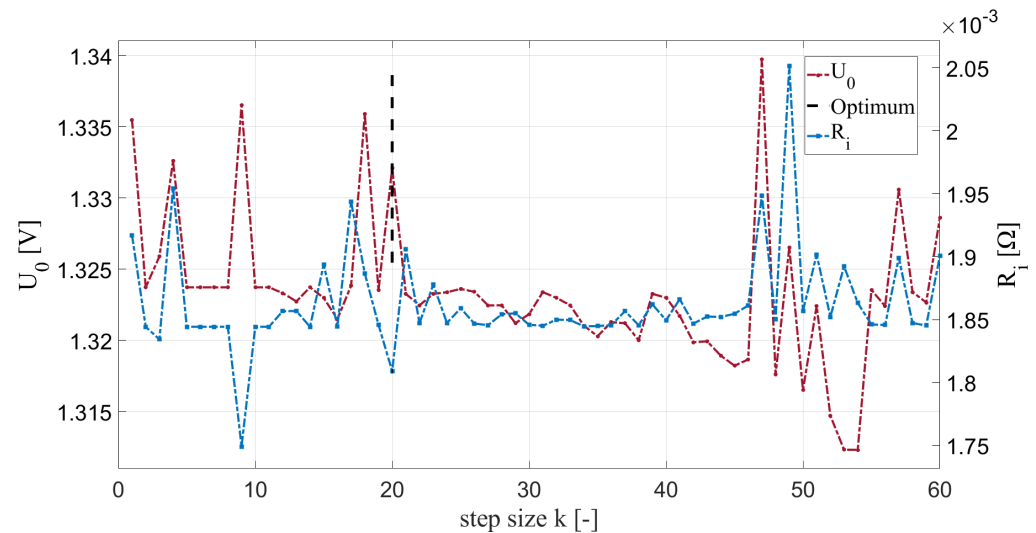


Figure 8. Third optimization step of U_0 and R_i with preset step size of $k = 60$.

3.3. Validation of the Simulation with Real Measurement

In order to be able to make conclusions about the quality of the simulation model, the measured data and the calculated data are compared in Figure 9. The stack voltages and the SOC, calculated by the simulation model, are shown in blue. The raw data are shown in green, which are directly derived from the measurement tests and were used for parameterization. This represents the final step of the validation and clearly visualizes the deviation between the model and the real data.

Regarding the stack voltages, it becomes apparent for all current curves that the simulation corresponds only very vaguely to the real measured data. Both curves are only slightly congruent or not congruent at all. However, the voltage curves over the entirety of the preset measurement voltages have one thing in common: the slope of the simulation lines is almost parallel to the CC phases of the charging processes. Thus, the assumption arises that the mathematical optimization routine is not suitable for the calculation of a charging process with CC and CV phase. More details are shown in the next figure, which illustrates the difference between simulated and measured data.

The influence of the current strength is essential for the amount of discrepancy between simulated and actual data [9]. This is where the real complexity of the Nernst equation becomes apparent. Linear and non-linear regions exist over the course of the voltage. During the discharge, mass transport phenomena occur at the transition of the electrolyte to the electrode [30]. These non-linearities are particularly noticeable in the range of 30 A and 35 A discharge cycles. There, the voltage decreases almost linearly to a value of 46.6 V. After that, a sharp drop in this value can be seen. The approximated simulated value is nevertheless linear, which represents a considerable discrepancy between simulation and real data. This further limits the scope for the application, and thus narrows the SOC limits. Zugschwert [9] assumes that no limiting current densities and extreme states of the voltage profile are reached near the SOC limitations limiting the prediction capabilities of the model.

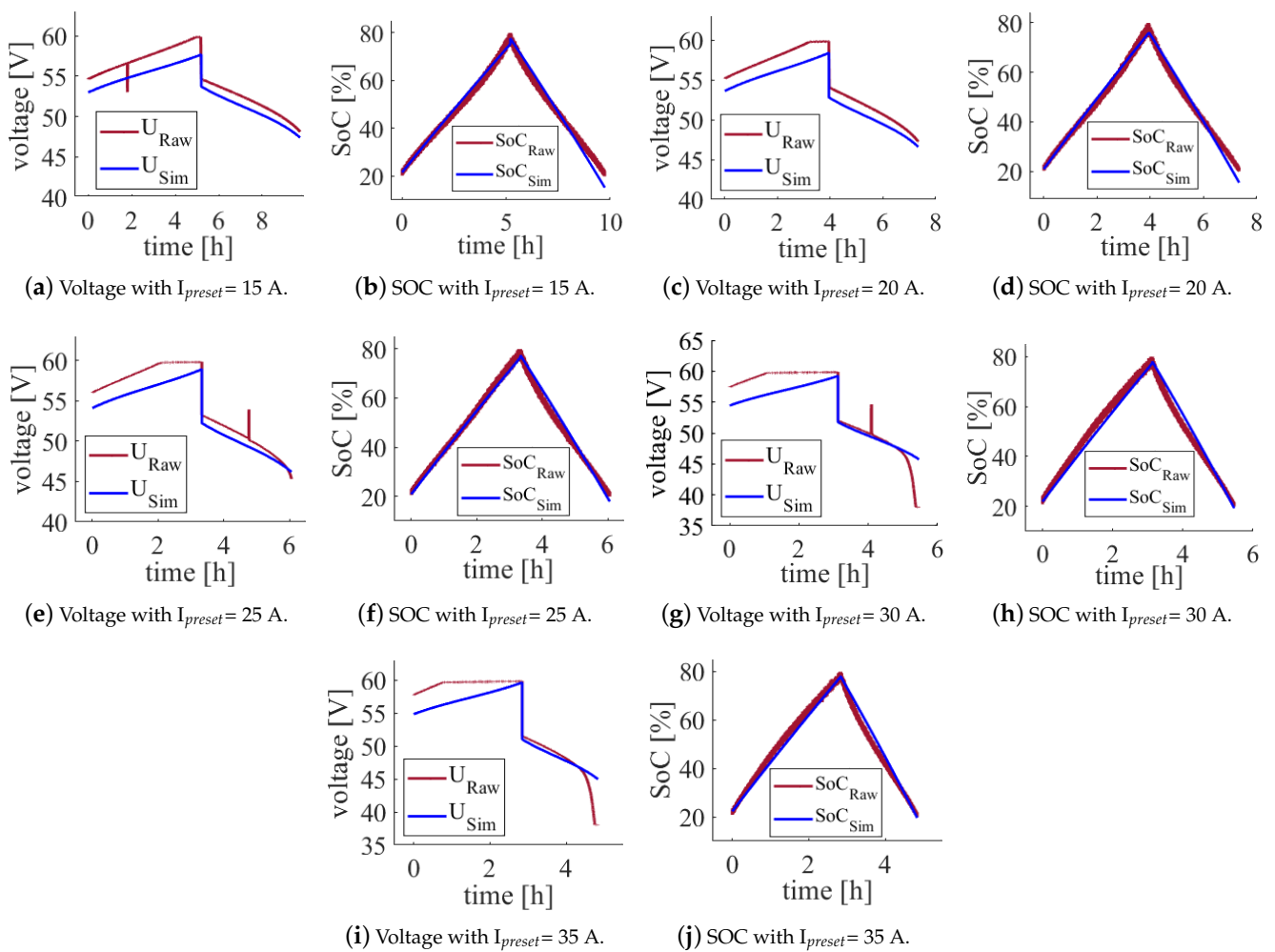


Figure 9. Comparison of the original raw data with the simulation data with preset current I_{preset} from 15 A to 35 A based on SOC and voltage.

Concerning the SOC, the simulated values almost completely map the progression of the measured data. Since the raw data are similar to a linear course, the previous assumption is confirmed that straight-line developments of the parameters can be reproduced much better.

Accordingly, the limits of the simulation model are as follows. At lower currents, the behavior between 20% and 80% can be reproduced very well. As the current increases, the accuracy of the model decreases towards the end of the discharge process due to increasing non-linearities in the voltage profile. The validity range is reduced to a SOC between 20% and around 70%. In order to be able to assess the discrepancy and its effects during the charging phase more accurately. The previously described assumption is examined to see how the accuracy between simulation and measured data differs when the horizontal voltage curve (CV phase) is removed. The modified measured data was then re-extracted, smoothed and parameterized. The result is illustrated and discussed in more detail below. All separate illustrations are shown in Figure 10.

Over all current levels, it becomes apparent in the CC range of the charging phase that the discrepancy increases with time. This is shown in Figure 11a from the beginning of each graph to their first maximum. The error here is between 1.73 V and 3.64 V. As already mentioned, this discrepancy increases with rising charge current, since the CV phase also becomes higher. The difference between simulation and measured data drops between 0 V and 2.3 V at the end of the charging phase. If the CV phase is reached during the charging process, its constant voltage value ensures a reduction of the deviation between model and

measured data. Since the calculated course of the voltage is almost linear, the measurement error also reduces with constant behavior.

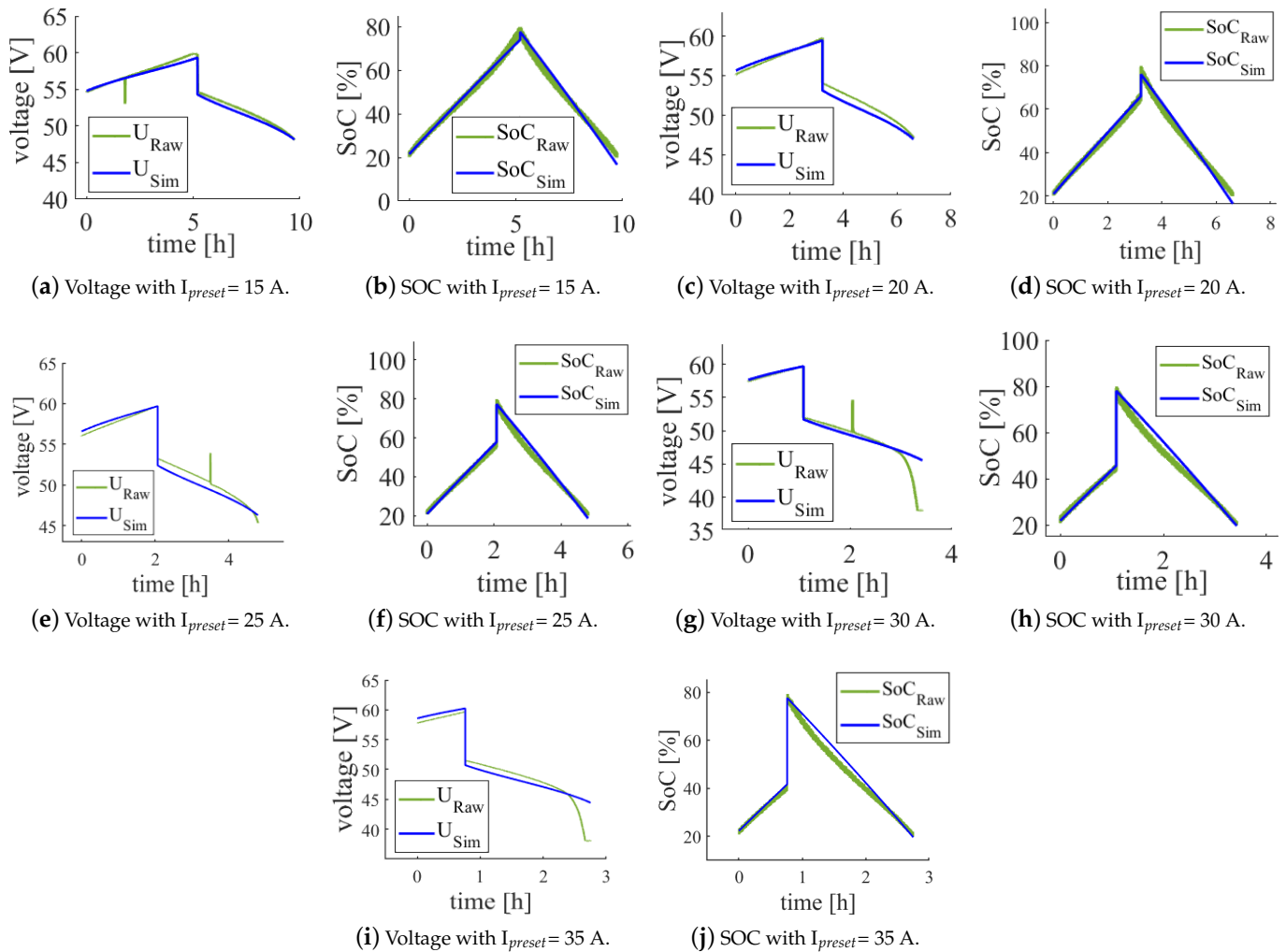
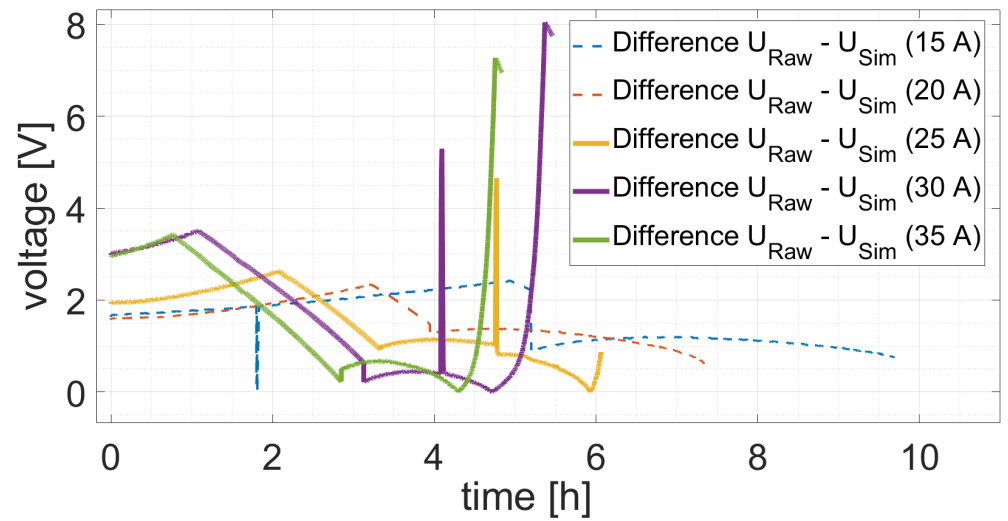


Figure 10. Comparison of raw data with simulation data with preset current I_{preset} from 15 A to 35 A based on SOC and voltage with CV phase excluded.

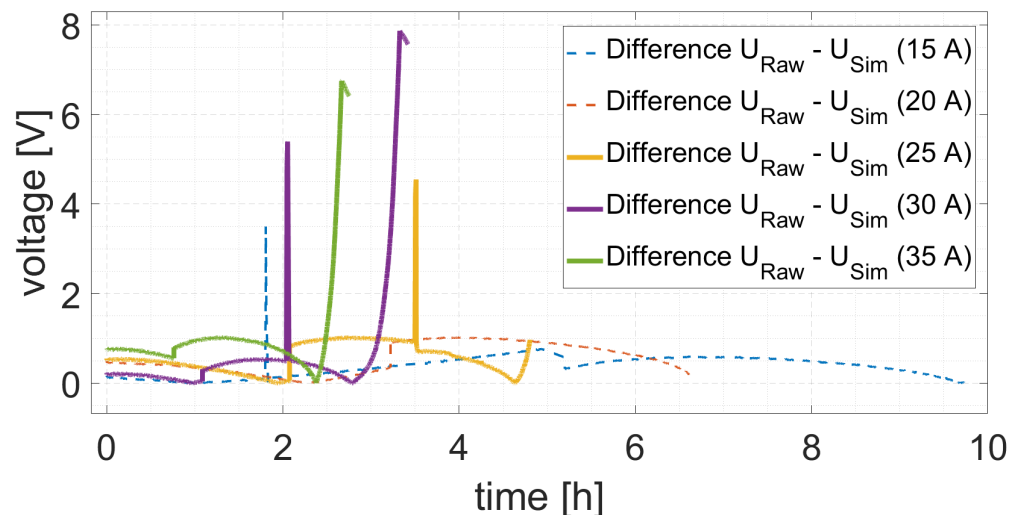
All curves show better results for the discharge cycles than for the charge cycles. However, this statement does not apply to the end of the discharge phase, since the voltage falls drastically at high discharge currents. The curves show a discrepancy of only 0 to 1.00 V, especially in the lower current range. Focusing on the end of the discharge phase at currents of 30 A and 35 A, the voltage drop explained above can only be represented very poorly in the model. The maximum deviation between the simulation model and the measured data is just over 8 V.

The difference between the measurement series and the simulation model are shown in Figure 11a,b. A time shift of the discharge cycles takes place by removing the CV phase of the in the charge cycle. The comparison between the errors in voltage prediction with and without CV phase clearly show that the discrepancy between simulation and raw data decreases. Thus, the error without CV phase is at a maximum of less than 1 V. Prior to this, it was at 3.64 V, which represents a discrepancy reduction of 72.5%. These results corroborate the conclusion that the simulation model can be parameterized less accurately with a CV phase. The previously mentioned discrepancy between raw data and simulation model at the end of the discharge process illustrates this effect. As this discrepancy depends on the linear approximation used in the model, non-linearities cannot be mapped adequately. At

discharge currents of 30 A and 35 A, the difference decreases with 0.17 V and 0.52 V, but increases by 0.1 A at discharge current of 25 A.



(a) Original Data.



(b) Modified data without CV phase.

Figure 11. Error deviation from the simulation model to the raw data with the: (a) original data; (b) modified data without CV phase.

Overall, the accuracy of the model without CV phase is similar to the results obtained in [9]. The deviation curve presented in the dissertation is very close to those in Figure 11b. Furthermore, with the data sets of Battery 2, the accuracy decreases at high currents towards the end of the discharge cycles. The same can be observed in the results with data sets of Battery 1. CV phases do not exist in the raw data of Battery 2 data because the upper cut-off voltage of 63 V is not reached [12]. As a result, the model is designed to have a linear approximation of the charge and discharge curve and shows inaccuracies associated with CV phases [1,9].

In order to evaluate the effects of removing the CV phase from the data set, the following Table 5 compares the optimization parameters.

Basically, the parameters C_{Stor} and U_0 do not show a large deviation between both parameterizations. The total capacity C_{Stor} decreases by 0.65 Ah (0.25%) without CV phase. The parameter U_0 decreases by 0.03 V, which corresponds to 2.21% when there is no CV phase in the data set. Larger deviations are shown for I_{Loss} , which is 0.41 A higher with CV

phase. This results in a difference of 9.67%. The situation is even higher for cell resistance R_i . This is 0.0006 Ω (25%) higher after parameterization with CV Phase than with the original data.

Table 5. Comparison of the optimization parameters with and without CV phase after parametrization.

	With CV Phase	Without CV Phase
Total capacity C_{Stor} [Ah]	255.66	255.01
Current loss I_{Loss} [A]	4.24	3.83
Cell voltage U_0 [V]	1.33	1.36
Cell resistance R_i [Ω]	0.0018	0.0024

4. Conclusions

Using the new data of a 5 kW VRFB, the simulation model proposed in [1] is validated. Differences in the experimental design between the new raw data (Battery 1) and the original measurements from [1] (Battery 2), make it impossible to use the model without modification. Thus, it has been identified that a universal approach for the experimental design is necessary to enable model functionality independent of the VRFB and BMS used.

As the model validation and optimization is based on the state variables current, voltage and SOC, these informations are essential. The SOC is not measured directly, but some VRFBs convert other data, e.g., OCV measurements within the BMS. In Battery 2 the SOC has been accessible via the BMS. Contrary, the BMS of Battery 1 did not calculate the SOC internally and only OCV data are measured during the cycles. For this purpose, possibilities are presented to calculate the SOC for VRFB systems and the usability of these methods is prioritized within the scope of this study.

Most suitable is the SOC–OCV relation, as OCV data has been recorded in high resolution during the measurement campaign of Battery 1. Although a linear relation between SOC and OCV has been reported in literature within defined borders, measurements from Battery 1 show an increasingly non-linear behavior at the SOC borders (20% and 80%) with increasing current. Starting with a linear regression, the SOC–OCV relation could not be mapped adequately for all currents. A polynomial regression is applied using all data sets and SOC–OCV conversion has been performed to enable further model validation.

Originally the simulation model was based on four modeling steps; **(i) raw data extraction, (ii) raw data modification, (iii) optimization and parameter fitting, and (iv) model validation.** The comparison and conversion of experimental design described above has been added as a raw data preparation step. After adapting the data set to the input schematics of the simulation model, the parameterization can be performed by calculating the four optimization parameters; I_{Loss} , C_{Stor} , R_i , and U_0 . Consecutive iteration loops lead to a minimal error between raw and simulated data for voltage, current, and SOC and associated optimization parameters are stored. In the last modeling step, time-dependent analysis of voltage, current, and SOC between the model and raw data is performed. Compared to the original modeling results from [1], raw data can be mapped inaccurately for all voltage profiles.

For this purpose, a new parameterization was carried by excluding the CV phase from the voltage raw data. As the original VRFB system was power-controlled, no CV phase has been present in [1]. The results show that the model represents the raw data sufficiently. As the mathematical description of the battery only map linear behavior, the transition from CC to CV phase in the voltage profile during charging lead to a parallel displacement and low accuracy of the model. During the discharge phase no CV has been present and the voltage profile can be mapped comparable to [1]. As already discussed in [1], non-linear voltage drops at the end of the discharge cycle cannot be mapped due to linear approximation.

The experimental design of two different VRFB systems has been analyzed to enable model functionality independent of the input data used. Besides stack voltage and current, the experimental design should either use OCV with subsequent SOC–OCV or conversion

or SOC values from the BMS. In case OCV measurements are used, it is recommended to clarify the electrolyte composition to avoid incorrect SOC assessment due to cross-over phenomena or irreversible side reactions. Moreover, power-controlled operation mode without transition from CC to CV phase improved model prediction. If current-controlled operation is present, it is recommended to separate CC and CV for adequate simulation of the voltage profile.

For future research, the differential-algebraic system can be improved to map the non-linear behavior of the battery at the end and beginning of the cycles. Additionally, the accuracy of the simulation model can be investigated if the CV phase is automatically removed and subsequently parameterized for the original data sets used. The analysis of electrochemical phenomena for the OCV–SOC behavior lies beyond the scope of this work and could be investigated within another study. The authors would recommend repeating the OCV measurements under different currents and in the best case to include electrolyte analysis to clarify and understand the parabolic trend and potential shifts in the electrolyte due to cross-over.

Author Contributions: Conceptualization, C.S., R.W., B.P. and K.-H.P.; methodology, C.S. and R.W.; software, C.S. and R.W.; validation, C.S., R.W. and B.P.; formal analysis, C.S. and R.W.; investigation, C.S. and R.W.; resources, C.S., R.W., B.P. and K.-H.P.; data curation, C.S., R.W. and B.P.; writing—original draft preparation, C.S. and R.W.; writing—review and editing, C.S., R.W., B.P. and K.-H.P.; visualization, C.S. and R.W.; supervision, C.S., B.P. and K.-H.P.; project administration, C.S., B.P. and K.-H.P.; funding acquisition, C.S., B.P. and K.-H.P. All authors have read and agreed to the published version of the manuscript.

Funding: This research is funded by the Horizon2020 research and innovation program of the European Union under grant agreement No 963550, HyFlow. This document reflects only the author’s view and the Agency is not responsible for any use that may be made of the information it contains. (HyFlow Grant Agreement, Art. 29.5 Disclaimer excluding Agency responsibility).

Data Availability Statement: The data presented in this study are available on request from the corresponding author. The data are not publicly available due to privacy.

Conflicts of Interest: The authors declare no conflict of interest. The funders had no role in the design of the study; in the collection, analyses, or interpretation of data; in the writing of the manuscript, or in the decision to publish the results.

Abbreviations

The following abbreviations are used in this manuscript:

CC	Constant Current
CV	Constant Voltage
BMS	Battery Management System
OCV	Open Circuit Voltage
RE	Renewable Energy
RFB	Redox Flow Battery
SOC	State of Charge
VRFB	Vanadium Redox Flow Battery

References

1. Zugschwert, C.; Dundálek, J.; Leyer, S.; Hadji-Minaglou, J.R.; Kosek, J.; Pettinger, K.H. The Effect of Input Parameter Variation on the Accuracy of a Vanadium Redox Flow Battery Simulation Model. *Batteries* **2021**, *7*, 7. [[CrossRef](#)]
2. Elavarasan, R.M.; Shafiullah, G.M.; Padmanaban, S.; Kumar, N.M.; Annam, A.; Vetrichelvan, A.M.; Mihet-Popa, L.; Holm-Nielsen, J.B. A Comprehensive Review on Renewable Energy Development, Challenges, and Policies of Leading Indian States with an International Perspective. *IEEE Access* **2020**, *8*, 74432–74457. [[CrossRef](#)]
3. Flannery, T.; Hughes, L.; Steffen, W.; Morgan, W.; Dean, A.; Smith, R.; Baxter, T. *From Paris to Glasgow: A World on the Move*; Climate Council: Sidney, Australia, 2021, ISBN 978-1-922404-37-4.
4. Aneke, M.; Wang, M. Energy storage technologies and real life applications—A state of the art review. *Appl. Energy* **2016**, *179*, 350–377. [[CrossRef](#)]
5. Maria, S.K.; Miron, R.; Robert, R. All-Vanadium Redox Battery. Patent number US4786567A, 11 February 1986.

6. Lucas, A.; Chondrogiannis, S. Smart grid energy storage controller for frequency regulation and peak shaving, using a vanadium redox flow battery. *Int. J. Electr. Power Energy Syst.* **2016**, *80*, 26–36. [[CrossRef](#)]
7. Viswanathan, V.; Crawford, A.; Stephenson, D.; Kim, S.; Wang, W.; Li, B.; Coffey, G.; Thomsen, E.; Graff, G.; Balducci, P.; et al. Cost and performance model for redox flow batteries. *J. Power Sources* **2014**, *247*, 1040–1051. [[CrossRef](#)]
8. Parasuraman, A.; Lim, T.M.; Menictas, C.; Skyllas-Kazacos, M. Review of material research and development for vanadium redox flow battery applications. *Electrochim. Acta* **2013**, *101*, 27–40. [[CrossRef](#)]
9. Christina Zugschwert. Evaluation von Synergieeffekten Zentraler Speichersysteme in Niederspannungsnetzen Durch Integrative Modellbildung. Ph.D. Thesis, Université du Luxembourg, Luxembourg, 2022.
10. Robert Labus. Teststandoptimierung für eine Vanadium-Redox-Flow-Batterie unter Einbezug der Erfassung thermischer und Elektrischer Systemparameter. Master's Thesis, Hochschule für angewandte Wissenschaften Landshut, Landshut, Germany, 2020.
11. Volterion GmbH. *Datenblatt—Vanadium Redox Flow Battery VRFB 11/12*; Volterion GmbH: Dortmund, Germany, 2018.
12. Gildemeister Energy Solutions. *Datenblatt—Vanadium Redox Flow Battery FB10-100*; Gildemeister Energy Solutions: Wiener Neudorf, Austria, 2012.
13. Wei, L.; Zhao, T.S.; Xu, Q.; Zhou, X.L.; Zhang, Z.H. In-situ investigation of hydrogen evolution behavior in vanadium redox flow batteries. *Appl. Energy* **2017**, *190*, 1112–1118. [[CrossRef](#)]
14. Piller, S.; Perrin, M.; Jossen, A. Methods for state-of-charge determination and their applications. *J. Power Sources* **2001**, *96*, 113–120. [[CrossRef](#)]
15. Skyllas-Kazacos, M.; Kazacos, M. State of charge monitoring methods for vanadium redox flow battery control. *J. Power Sources* **2011**, *196*, 8822–8827. [[CrossRef](#)]
16. Knehr, K.W.; Kumbur, E.C. Open circuit voltage of vanadium redox flow batteries: Discrepancy between models and experiments. *Electrochem. Commun.* **2011**, *13*, 342–345. [[CrossRef](#)]
17. Corcuera, S.; Skyllas-Kazacos, M. State-of-Charge Monitoring and Electrolyte Rebalancing Methods for the Vanadium Redox Flow Battery. *Eur. Chem. Bull.* **2012**, *1*, 511–519. [[CrossRef](#)]
18. König, S. Model-Based Design and Optimization of Vanadium Redox Flow Batteries. Ph.D. Thesis, Karlsruher Institut für Technologie, Karlsruhe, Germany, 2017. [[CrossRef](#)]
19. Fathima, A.H.; Palanisman, K. Modeling and Operation of a Vanadium Redox Flow Battery for PV Applications. *Energy Procedia* **2017**, *117*, 607–614. [[CrossRef](#)]
20. Shin, K.H.; Jin, C.S.; So, J.Y.; Park, S.K.; Kim, D.H.; Yeon, S.H. Real-time monitoring of the state of charge (SOC) in vanadium redox-flow batteries using UV-Vis spectroscopy in operando mode. *J. Energy Storage* **2020**, *27*, 101066. [[CrossRef](#)]
21. Hudak, N.S. Practical thermodynamic quantities for aqueous vanadium- and iron-based flow batteries. *J. Power Sources* **2014**, *269*, 962–974. [[CrossRef](#)]
22. Bard, A.J.; Faulkner, L.R. *Electrochemical Methods: Fundamentals and Applications*, 2nd ed.; Wiley: New York, NY, USA; Weinheim, Germany, 2001.
23. Guidelli, R.; Piccardi, G.; Moncelli, M.R. Mechanism of electrohydrodimerization of deactivated olefins in aqueous media. *J. Electroanal. Chem. Interfacial Electrochem.* **1981**, *129*, 373–378. [[CrossRef](#)]
24. Wei, Z.; Lim, T.M.; Skyllas-Kazacos, M.; Wai, N.; Tseng, K.J. Online state of charge and model parameter co-estimation based on a novel multi-timescale estimator for vanadium redox flow battery. *Appl. Energy* **2016**, *172*, 169–179. [[CrossRef](#)]
25. Mohamed, M.R.; Leung, P.K.; Sulaiman, M.H. Performance characterization of a vanadium redox flow battery at different operating parameters under a standardized test-bed system. *Appl. Energy* **2015**, *137*, 402–412. [[CrossRef](#)]
26. Noack, J.; Wietschel, L.; Roznyatovskaya, N.; Pinkwart, K.; Tübke, J. Techno-Economic Modeling and Analysis of Redox Flow Battery Systems. *Energies* **2016**, *9*, 627. [[CrossRef](#)]
27. Huang, Z.; Mu, A. Research and analysis of performance improvement of vanadium redox flow battery in microgrid: A technology review. *Int. J. Energy Res.* **2021**, *45*, 14170–14193. [[CrossRef](#)]
28. Zhang, Y.; Zhao, J.; Wang, P.; Skyllas-Kazacos, M.; Xiong, B.; Badrinarayanan, R. A comprehensive equivalent circuit model of all-vanadium redox flow battery for power system analysis. *J. Power Sources* **2015**, *290*, 14–24. [[CrossRef](#)]
29. Kim, S.; Thomsen, E.; Xia, G.; Nie, Z.; Bao, J.; Recknagle, K.; Wang, W.; Viswanathan, V.; Luo, Q.; Wei, X.; et al. 1 kW/1 kWh advanced vanadium redox flow battery utilizing mixed acid electrolytes. *J. Power Sources* **2013**, *237*, 300–309. [[CrossRef](#)]
30. Bard, A.J.; Faulkner, L.R.; White, H.S. *Electrochemical Methods: Fundamentals and Applications*, 3rd ed.; Wiley: Hoboken, NJ, USA, 2022.

Disclaimer/Publisher's Note: The statements, opinions and data contained in all publications are solely those of the individual author(s) and contributor(s) and not of MDPI and/or the editor(s). MDPI and/or the editor(s) disclaim responsibility for any injury to people or property resulting from any ideas, methods, instructions or products referred to in the content.